Biomass chitosan-deriving Co-induced N-doped carbon nanotubes to support Mn_3O_4 as efficient electrocatalysts for Rechargeable Zn-air Battery

Wenshu Zhou [a, b, e], Yanyan Liu [a, c, d], Dichao Wu [a], Limin Zhou[d], Gaoyue Zhang [a], Kang Sun [a], Baojun Li [d], Jianchun Jiang [a, b, *]

[a] Institute of Chemical Industry of Forest Products, Chinese Academy of Forestry (CAF), National Engineering Lab. for Biomass Chemical Utilization, Key and Open Lab. of Forest Chemical Engineering, SFA, Nanjing, Jiangsu Province, 210042, China

[b] Co-Innovation Center of Efficient Processing and Utilization of Forest Resources, Nanjing Forestry University, Nanjing, China

[c] College of Science, Henan Agricultural University, Zhengzhou, China

[d] College of Chemistry and Molecular Engineering, Zhengzhou University, Zhengzhou, China

[e] College of Food Science and Engineering, Nanjing University Of Finance & Economics, Nanjing, China

* Corresponding Author. E-mail: jiangjc@icifp.cn (J.C. Jiang)

Experimental section

Experimental section

Materials

Chitosan (deacetylation degree of 85%, and purity 99.5%), Cobalt(II) Acetate Tetrahydrate ($Co(Ac)_2.4H_2O$, 99%), Manganese(II) Acetate Tetrahydrate ($Mn(Ac)_2.4H_2O$, 99%) and other chemicals (analytically pure) were obtained from Aladdin Reagent, and used as received without further purification.

Synthesis of Co@NCNTs

In a typical process of synthesizing Co@NCNTs, 1 g of chitosan was dissolved in 100 mL of 2% acetic acid solution followed by adding 80 mg of $Co(Ac)_2$ and 10 g of urea under stirring to achieve a uniform mixture. The uniform mixture was dried and transferred into a covered crucible, heated in a quartz tube under a protective argon flow of 80 sccm, and annealed at a desired temperature for 2 h, the temperature increasing at the rate of 10 °C min^{-1}, followed by natural cooling to room temperature. NCS was synthesized without adding $Co(Ac)_2$, and CS was synthesized without adding urea and $Co(Ac)_2$.

Synthesis of Mn_3O_4/NCNTs@Co

$Mn(Ac)_2{\cdot}4H_2O$ (0.05 g) and Co@NCNTs (0.08 g) were ultrasonically dissolved in 50 mL of deionized water and sonicated for 20 min. Then $NH_3{\cdot}H_2O$ (665 μL) was added by drop-wise. This mixture was transferred into an autoclave and heated at 180 °C for 12 h. After the reaction, the product was collected by filtration and washed with ultrapure water and ethanol 3 times. The final Mn_3O_4/NCNTs@Co was obtained by freeze-drying the precipitates. To illustrate the effect of cobalt and Mn_3O_4 doping on the electrocatalytic activity, NCS-supported pristine Mn_3O_4 nanocrystals was synthesized by the same process.

Characterization

Transmission electron microscopy (TEM) images were collected from JEOL-JEM-2100 with elemental mappings collected by EDAX. The crystal structure of products were was identified by X-ray diffraction (XRD) using a Brüker D8 advance with Cu Kα radiation (λ= 1.5418 Å). Raman spectra was obtained on a Renishaw RM-1000 with Ar-ion laser (λ=514 nm). X-ray photoelectron spectroscopy (XPS) was investigated on the Thermo Scientific K-Alpha+ with Al Kα X-ray as the excitation source. N_2 sorption isotherms were measured on a urface area and porosity analyzer (Micrometrics Tristar 3020 s) at 77.35 K.

All the electrochemical tests were carried out on a CHI 760E electrochemical workstation (CH Instruments, Inc, Shanghai) equipped with a rotating ring-disk electrode (RRDE) system in a standard three-electrode system with KOH as the electrolyte a platinum wire as the counter electrode, Hg/HgO electrode as the reference electrode and a modified glassy carbon electrode as the working electrode. All the measured potentials were calibrated relative to the reversible hydrogen electrode (RHE) according to the following calculation:

$$E_{RHE} = E_{Hg/HgO} + 0.098 + 0.059pH \qquad (1)$$

The working electrodes were prepared as follows: 4 mg of the electrocatalyst was dispersed into a mixed solvent containing with ethanol and nafion (v/v=720/80) to form the homogeneous dispersion by ultrasonication treatment for 60 min. Then, 10 μL of the above solution was pipetted onto a polished glassy-carbon rotating risk electrode and dried at room temperature. The cyclic voltammetric (CV) measurements was performed in O_2/N_2-saturated 0.1 M KOH until obtaining a stable profile. Then, the linear sweep voltammetry (LSV) curves were measured to evaluate ORR or OER activity, respectively. The presented current density was normalized to the geometric surface area of electrodes. The poison

tests for ORR were performed in mixed solution containing KOH (0.1 M) and CH_3OH (1 M). Rotating ring disk electrode (RRDE) measurements were carried out in O_2-saturated KOH (0.1 M) at 1600 rpm with a scan rate of 5 mV s^{-1}, and the potential of the Pt ring was set at 1.3 V (vs RHE). The yield of H_2O_2 and the electron transfer number (*n*) were calculated by the following equation:

$$n = \frac{4I_D}{I_D + I_R / N} \quad (2)$$

$$[H_2O_2]\% = \frac{200I_R / N}{I_R / N + I_D} \quad (3)$$

where I_D and I_R are the disk and ring currents, respectively. N is the collection coefficient at the ring in RRDE experiments (N=0.37).

A home-made aqueous rechargeable Zn-air battery were assembled with a polished Zn plate (thickness: 0.3 mm, area: 1 cm^2) as the anode, carbon paper with catalyst-coated as the air cathode, and a 6.0 M KOH + 0.2 M $Zn(CH_3COO)_2 \cdot 2H_2O$ mixed solution as the electrolyte. The discharge/charge cycling of rechargeable Zn-air batteries were using recurrent galvanostatic pulses for 10 min of charge followed by 10 min of discharge at 5 mA cm^{-2}. Polarization curve measurements (*v-i*) were performed by LSV at a scan rate of 10 mV s^{-1}. The current and power density curves were calculated from the LSV curves. All tests are performed in a natural environment.

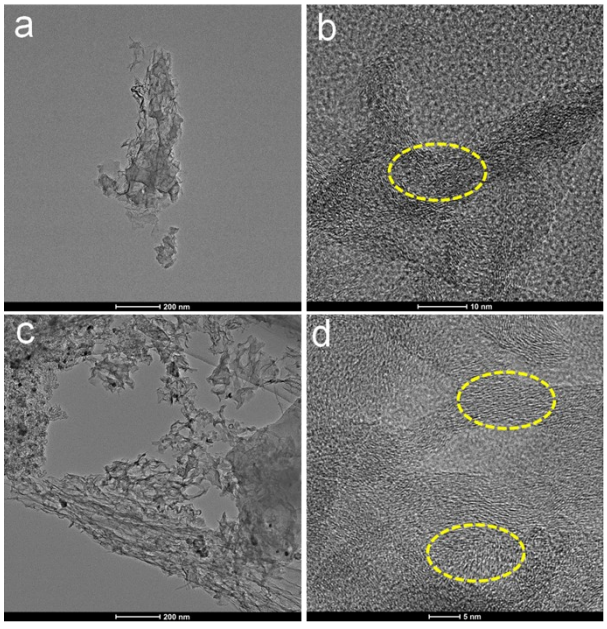

Figure S1. (a-b) TEM and HRTEM images of CS, (c-d) TEM and HRTEM images of NCS

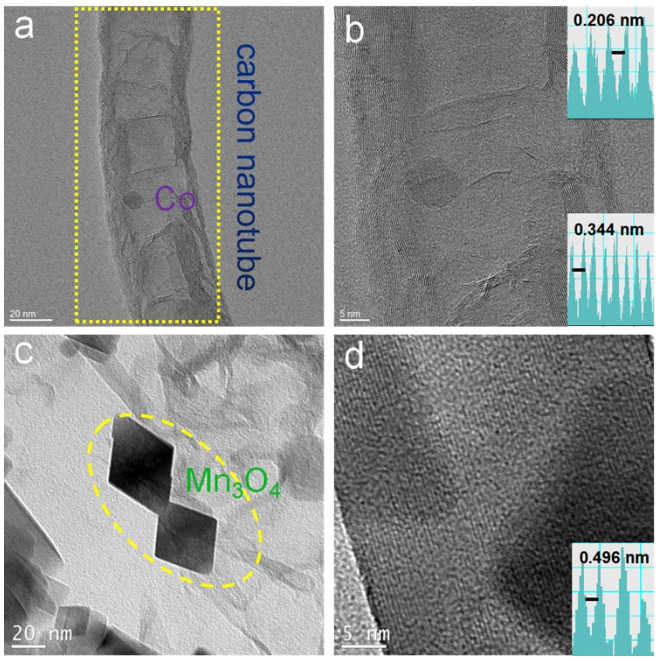

Figure S2. (a-b) TEM and HRTEM images of Co@NCNTs (including the corresponding atomic intensity profifiles), (c-d) TEM and HRTEM images of Mn_3O_4/NCS (including the corresponding atomic intensity profifiles)

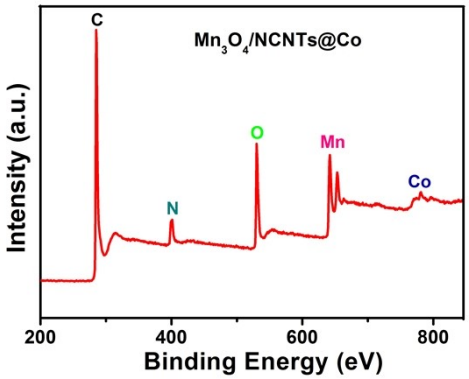

Figure S3. Survey spectrum of Mn_3O_4/NCNTs@Co

Table S1. The *t*-Plot report of CS, NCS, Co@NCNTs, Mn_3O_4/NCS and Mn_3O_4/NCNTs@Co.

t-Plot report	average pore-size	specific surface area	pore volume
	nm	$m^2\ g^{-1}$	$cm^3\ g^{-1}$
CS	2.8	289	1.08
NCS	2.5	338	1.33
Co@NCNTs	2.3	167.6	0.62
Mn_3O_4/NCS	2.4	179.8	0.56
Mn_3O_4/NCNTs@Co	2.1,	123.5	0.37

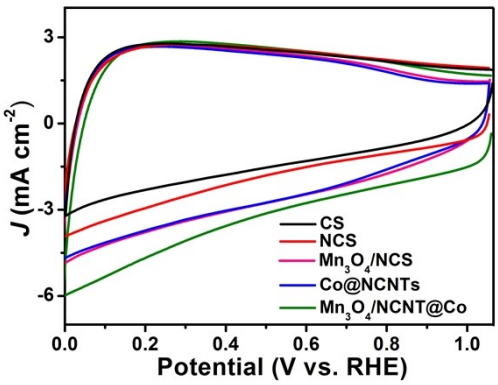

Figure S4. CV curves of CS, NCS, Co@NCNTs, Mn_3O_4/NCS and Mn_3O_4/NCNTs@Co in Ar_2-saturated 0.1 M KOH

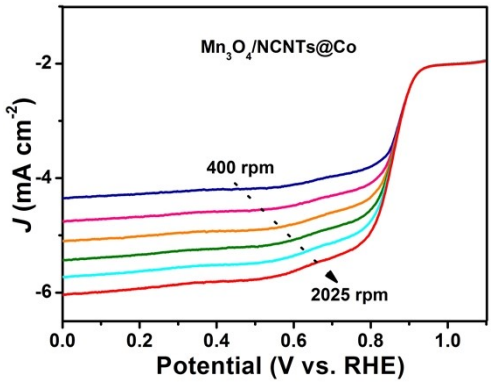

Figure S5. LSV curves of Mn_3O_4/NCNTs@Co at different rotating rates.

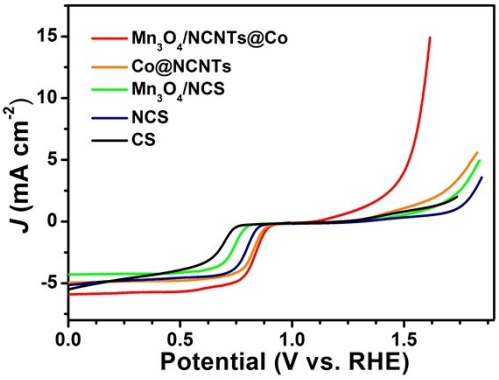

Figure S6. LSV curves of CS, NCS, Co@NCNTs, Mn_3O_4/NCS and Mn_3O_4/NCNTs@Co at 1800 rpm, showing the electrocatalytic activities for ORR and OER.

Table S2 . the comparison of ORR, OER and dual catalytic performances in this work to some results from literatures.

Sample	$E_{ORR\ onset}$ **[V]**	$E_{ORR1/2}$ **[V]**	**Transferred electrons (*n*)**	E_{OER}**[V] (j=10 mA cm^{-2})**	**ΔE ($E_{j=10}$ - $E_{1/2}$)(V)**	**RZABs cycle Duration [h]**	**Ref.**
Mn_3O_4@HCM	0.75	0.68	3.95	-	-	115	S1
Mn_3O_4/O-CNTs	0.92	0.85	3.95	1.65	0.80	160	S2
Mn_3O_4/N-CNT/GDL	0.85	0.70	-	-	-	100	S3
$Mn_3O_4/NiCo_2S_4$	0.92	0.81	3.99	1.55	0.74	217	S4
Ni-doped Mn_2O_3	0.935	0.80	3.986	-	-	50	S5
Co_3O_4/Mn_3O_4/N-rGO	0.92	0.86	3.96	1.59	0.73	400	S6
Mn_3O_4@$CoMn_2O_4$-Co_xO_y	0.90	0.81	3.5	1.75	0.94	-	S7
Mn_3O_4/NCNTs@Co	0.92	0.85	~4.0	1.53	0.68	366	**This work**

References:

S1. Y.J. He, D. Aasen, H.Y. Yu, M. Labbe, D.G. Ivey, J.G.C. Veinot, Mn_3O_4 nanoparticle-decorated hollow mesoporous carbon spheres as an efficient catalyst for oxygen reduction reaction in Zn-air batteries, Nanoscale Adv. 2 (2020) 3367-3374.

S2. L.Q. Li, J. Yang, H.B. Yang, L.P. Zhang, J.J. Shao, W. Huang, B. Liu, X.C. Dong, Anchoring Mn_3O_4 nanoparticles on oxygen functionalized carbon nanotubes as bifunctional catalyst for rechargeable Zinc-air battery, ACS Appl. Energy Mater. 1 (2018) 963-969.

S3. D. Aasen, M. Clark, D.G. Ivey, A gas diffusion layer impregnated with Mn_3O_4-decorated N-doped carbon nanotubes for the oxygen reduction reaction in Zinc-air Batteries, Batteries & Supercaps. 2 (2019) 882-893.

S4. F.B. Wang, G.D. Li, X.G. Meng, S.J. Xu, W.Q. Ma, One-dimensional $Mn_3O_4/NiCo_2S_4$ nanocomposites as high-performance bifunctional electrocatalyst for rechargeable liquid/flexible Zn-air batteries, J. Power Sources. 462 (2020) 228162.

S5. H. Kim, K. Min, S.E. Shim, D. Lim, S.-H. Ni-doped Mn_2O_3 microspheres as highly effificient electrocatalyst for oxygen reduction reaction and Zn-air battery, Int. J. Hydrogen energy. 47 (2022) 2378-2388.

S6. Q.K. Huang, X.W. Zhong, Q. Zhang, X. Wu, M.L. Jiao, B. Chen, J.Z. Sheng, G.M. Zhou, Co_3O_4/Mn_3O_4 hybrid catalysts with heterointerfaces as bifunctional catalysts for Zn-air batteries, J. Energy Chem. 68 (2022) 679-681.

S7. Z.H. Luo, E. Irtem, M. Ibáñez, R. Nafria, S. Martí-Sánchez, A. Genç, M. Mata, Y. Liu, D. Cadavid, J. Llorca, J. Arbiol, T. Andreu, J.R. Morante, A. Cabot, Mn_3O_4@$CoMn_2O_4$-Co_xO_y nanoparticles: partial cation exchange synthesis and electrocatalytic properties toward the oxygen reduction and evolution reactions, ACS Appl. Mater. Interfaces. 8 (2016) 17435-17444.